ARTICLE OPEN

Check for updates

Commensurate-to-incommensurate transition of charge-density-wave order and a possible quantum critical point in pressurized kagome metal CsV_3Sb_5

X. Y. Feng[1,2], Z. Zhao[1,2], J. Luo[1], J. Yang[1], A. F. Fang[3], H. T. Yang[1,2,4], H. J. Gao[1,2,4,5], R. Zhou[1,4]✉ and Guo-qing Zheng[6]

Clarifying the interplay between charge-density waves (CDWs) and superconductivity is important in the kagome metal CsV_3Sb_5, and pressure (P) can play a crucial role. Here, we present $^{121/123}$Sb nuclear quadrupole resonance (NQR) measurements under hydrostatic pressures up to 2.43 GPa in CsV_3Sb_5 single crystals. We demonstrate that the CDW gradually changes from a commensurate modulation with a star-of-David (SoD) pattern to an incommensurate one with a superimposed SoD and Tri-hexagonal (TrH) pattern stacking along the c-axis. Moreover, the linewidth $\delta\nu$ of $^{121/123}$Sb-NQR spectra increases with cooling down to T_{CDW}, indicating the appearance of a short-range CDW order due to CDW fluctuations pinned by quenched disorders. The $\delta\nu$ shows a Curie–Weiss temperature dependence and tends to diverge at $P_c \sim 1.9$ GPa, suggesting that a CDW quantum critical point (QCP) exists at P_c where T_c shows the maximum. For $P > P_c$, spin fluctuations are enhanced when the CDW is suppressed. Our results suggest that the maximal T_c at $P_c \sim 1.9$ GPa is related to the CDW QCP, and the presence of spin fluctuations prevents the T_c from a rapid decrease otherwise, after the CDW is completely suppressed.

npj Quantum Materials (2023)8:23 ; https://doi.org/10.1038/s41535-023-00555-w

INTRODUCTION

Unconventional superconductivity always arises in the vicinity of another ordered electronic state, such as a magnetic order[1], a nematic order[2], or even a charge-density wave (CDW)[3]. In cuprate high-temperature superconductors, iron-pnictides or heavy-fermion compounds, carrier dopings or externally applied pressures can suppress the magnetic or nematic order[4–6]. Quantum critical points (QCPs) and associated fluctuations were often found around the ending point of these orders and considered by many a key to understanding the mechanism of unconventional superconductivity[1,7–10]. However, unconventional superconductivity around a CDW QCP is rarely observed[11], and whether CDW fluctuations can also mediate the electron pairing is still a mystery.

Recently, a newly discovered quasi-two-dimensional superconductor AV_3Sb_5 (A = K, Cs, Rb) with kagome lattice has emerged as an excellent platform to study the interplay between topology, superconductivity, and CDW[12]. Angle-resolved photoemission spectroscopy combined with density-functional theory reveals a series of non-trivial electronic structures in this compound, including flat band, Dirac point, Van Hove singularity, and topological surface states[13–18]. Meanwhile, many exotic features, including chirality[19–23], nematicity[24], and time-reversal symmetry-breaking[25,26], were found in the CDW state, which was proposed to be driven by electron correlations[27,28]. Especially the unusual phase diagram of the CDW order and superconductivity with applying hydrostatic pressures attracted a lot of attention[29–32]. The CDW transition can be gradually suppressed by applying hydrostatic pressure until $P_c \sim 1.9$ GPa, and the superconducting transition temperature T_c shows a non-monotonic double-dome-like phase diagram until its disappearance around 10 GPa[31–34]. Most remarkably, the maximum T_c is right at P_c, where no Hebel–Slichter coherence peak is seen below T_c in the superconducting state[35]. All these studies point to a possible QCP at P_c[36,37], which makes CsV_3Sb_5 an ideal compound to study the relationship between unconventional superconductivity and CDW. Although the high-pressure nuclear magnetic resonance (NMR) experiments suggested that the CDW undergoes an evolution to a new phase with a possible stripe-like CDW order with a unidirectional $4a_0$ modulation in pressurized CsV_3Sb_5[35], information about pressure-dependent CDW fluctuations is still lacking, which is of much significance to clarify its interaction with superconducting symmetry. Besides the CDW fluctuations, spin fluctuations were also proposed to play an important role in the high-pressure superconducting phase[36,38]. But whether spin fluctuations exist or not and how they are affected by pressures are still unclear in the current stage.

RESULTS AND DISCUSSIONS

Commensurate-to-incommensurate transition of the CDW order

Figure 1 shows the crystal structure and the temperature dependence of AC susceptibility measured at various pressures by using an in situ NMR coil. The strong diamagnetic signal and the sharp superconducting transition are observed at $P = 0.40$ GPa and $P \geq 1.90$ GPa, indicating the high quality of the sample. As in previous studies, the much broader superconducting transitions are observed at $0.84\ \text{GPa} \leq P \leq 1.72$ GPa[31,32]. The obtained pressure dependence of T_c is consistent with previous transport studies (see Supplementary Fig. 3).

[1]Institute of Physics, Chinese Academy of Sciences, and Beijing National Laboratory for Condensed Matter Physics, 100190 Beijing, China. [2]School of Physical Sciences, University of Chinese Academy of Sciences, 100190 Beijing, China. [3]Department of Physics, Beijing Normal University, 100875 Beijing, China. [4]Songshan Lake Materials Laboratory, 523808 Dongguan, Guangdong, China. [5]CAS Center for Excellence in Topological Quantum Computation, University of Chinese Academy of Sciences, 100190 Beijing, China. [6]Department of Physics, Okayama University, Okayama 700-8530, Japan. ✉email: rzhou@iphy.ac.cn

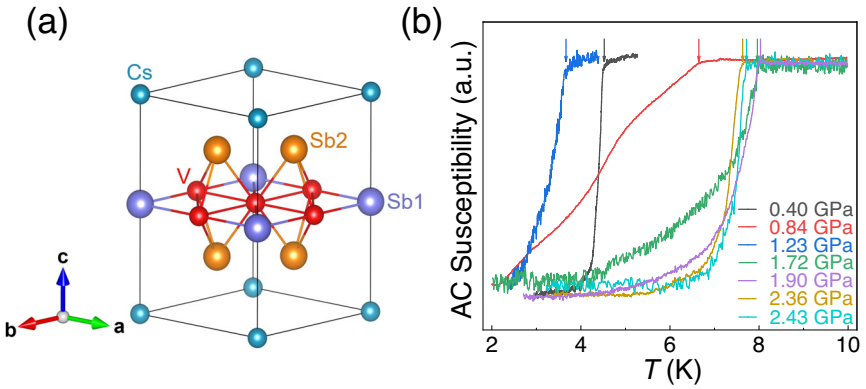

Fig. 1 The crystal structure and AC susceptibility measurements. a The pristine crystal structure of CsV_3Sb_5 at ambient pressure. **b** The temperature dependence of the AC susceptibility measured by using an in situ NQR coil at various pressures from 0.40 to 2.43 GPa. Solid arrows represent the superconducting transition temperature T_c.

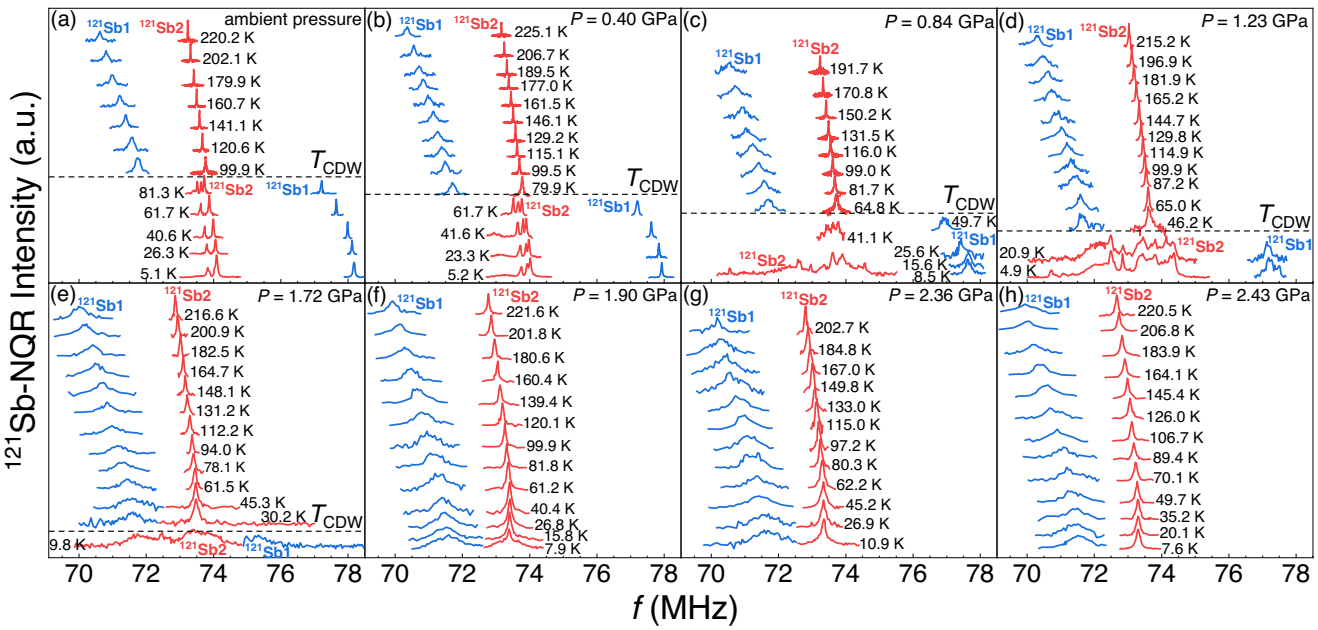

Fig. 2 Temperature-dependent NQR spectra. a–h represent the temperature dependence of ^{121}Sb1 (blue color) and ^{121}Sb2 (red color) NQR spectra at various pressures. The black dotted line indicates the temperature where the CDW phase transition occurs.

There are two types of Sb sites in CsV_3Sb_5. Sb1 is located in the kagome plane surrounded by the vanadium hexagon, and Sb2 is located between the kagome plane and Cs layer as illustrated in Fig. 1a. Sb has two types of isotopes, ^{121}Sb ($I = 5/2$) and ^{123}Sb ($I = 7/2$). The quadrupole frequency ν_q is defined as $\nu_q = \frac{3e^2qQ}{2I(2I-1)h}$, where eq is the electric field gradient (EFG), and Q is the nuclear quadrupole moment. For ^{121}Sb nucleus, the NQR spectrum should have two resonance peaks corresponding to $\pm 1/2 \leftrightarrow \pm 3/2$ and $\pm 3/2 \leftrightarrow \pm 5/2$ transitions. For ^{123}Sb nucleus, the NQR spectrum should have three resonance peaks corresponding to $\pm 1/2 \leftrightarrow \pm 3/2$, $\pm 3/2 \leftrightarrow \pm 5/2$ and $\pm 5/2 \leftrightarrow \pm 7/2$ transitions. So a total of 10 lines should be observed in $^{121/123}$Sb-NQR spectrum for CsV_3Sb_5, which is indeed seen in previous NQR studies[28,39]. Figure 2 displays the temperature dependence of ^{121}Sb-NQR spectra corresponding to $\pm 1/2 \leftrightarrow \pm 3/2$ transitions at various pressures. For all pressures, there is only one peak for both ^{121}Sb1 and ^{121}Sb2 above T_{CDW}. For $P < 1.9$ GPa, a clear change of the Sb-NQR spectrum due to the CDW transition can be seen as observed at ambient pressure[28,39], but T_{CDW} gradually decreases with increasing pressure. The abrupt jump of the Sb1 line was observed until $P = 1.23$ GPa, indicating the CDW order is of the first order. But it is hard to determine the type of the CDW transition for $P = 1.72$ GPa, since the line is too broad in the CDW state (see Supplementary Fig. 5).

Inside the CDW state, we further found that the line shape of ^{121}Sb2-NQR spectra experienced a remarkable change with increasing pressure, as shown in Fig. 3. For $P \leq 0.4$ GPa, a simple splitting of ^{121}Sb2 lines was observed, indicating that the CDW order is still commensurate and the lattice distortion should be still star-of-David (SoD) pattern[28]. With increasing pressure, at $P = 0.84$ GPa, both Sb1 and Sb2-NQR lines start to broaden, and new lines emerge at low frequencies. Below $P = 1.23$ GPa, some sharp lines can still be seen between $f = 72$ MHz to 75 MHz, but only broad lines remain at $P = 1.72$ GPa.

The observed broadening and emergence of new lines imply that the CDW modulation is totally different from the modulation at ambient pressure. Below we show that an incommensurate (IC) CDW order with superimposed SoD and TrH pattern stacking along the c-axis can consistently account for the observed results. Generally speaking, in a commensurate CDW state, the NQR line reflects the small number of physically non-equivalent nuclear sites in the unit cell so that the spectrum with discrete peaks was observed. In an

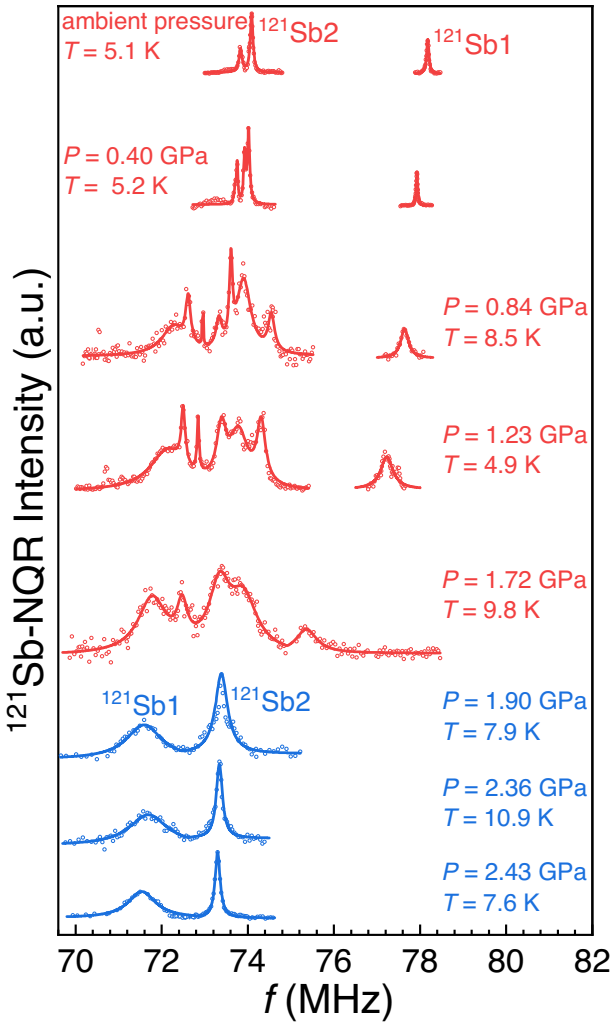

Fig. 3 Pressure evolution of NQR spectra. The red peaks are ^{121}Sb-NQR spectra in the CDW state at $T \sim T_c$ from ambient pressure to 1.72 GPa. The blue peaks are the ^{121}Sb-NQR spectra at $T \sim T_c$ above $P = 1.90$ GPa. The solid lines are the guides to the eye.

incommensurate state, however, since the translational periodicity is lost, the number of non-equivalent nuclear sites becomes much larger and leads to a larger broadening[40]. A modulation due to CDW order will cause an additional term in the resonance frequency at the Sb site (x, y). In our model, we consider both one-dimensional (1D) and two-dimensional (2D) incommensurate modulations. In the 1D case, we assume that the charge modulation along one in-plane direction is incommensurate and introduce an additional cosine function as $\cos(\frac{2\pi}{a} q_x \cdot x)$[40]. In the 2D case, we assume that the incommensurate modulation is in-plane and introduce an additional term as $\cos(\frac{2\pi}{a} q_x \cdot x) + \cos[\frac{2\pi}{b}(q_y \cdot x \cdot \cos\beta + q_y \cdot y \cdot \sin\beta)]$[40]. q_x and q_y are the wave vectors along a and b-axis, respectively. β is the angle between the two in-plane wave vectors q_x and q_y, which is $\pi/3$ for the kagome lattice studied in this work. For the 1D incommensurate case, we propose that the SoD and TrH patterns could be either superimposed, as illustrated in Fig. 4a[41], or formed two different domains, as illustrated in Fig. 4b. For the 2D incommensurate case, we assume an additional charge modulation on top of the superimposed SoD and TrH pattern, either along the a-axis or c-axis, as illustrated in Fig. 4d, e. By only considering the structural distortion in the plane and convoluting with a Lorentz function (details about NQR spectra simulation are present in Supplementary Note 5), we can reproduce the spectra at $P = 1.72$ GPa for both 1D and 2D incommensurate modulation as shown in Fig. 4c, f, respectively.

However, for the 1D incommensurate modulation, the Sb1 NQR spectra should have two peaks of equal intensities at 74.5 and 75.4 MHz, respectively (see Fig. 4c), which is not observed at $P = 0.84$ GPa or 1.23 GPa (see Fig. 3). We note that a stripe CDW order was proposed by the previous ^{51}V-NMR study[35], which is similar to our assumption of the additional modulation along the a-axis. However, the incommensurability of CDW and the coexistence of SoD and TrH patterns were not caught by the ^{51}V-NMR. This might be because Sb nuclei are sensitive to charge modulation from the Sb 5p-orbitals, which was suggested to be different from the CDW originated from the V 3d-orbitals[42]. In addition, $^{121/123}$Sb-NQR spectra were found to have a much larger response to the CDW order compared to the ^{51}V-NMR spectra[28,39]. In any case, our results suggest that CDW modulation gradually changes from the commensurate CDW at ambient pressure to the incommensurate CDW with increasing pressure. However, the NMR line shape is independent of the value of the CDW wave vector q for incommensurate modulations. Moreover, the present experimental results do not rule out the possibility of more complex CDW patterns beyond the proposed structures in Fig. 4. To further resolve this issue, high-pressure X-ray scattering measurements at 1.72 GPa are needed in the future.

In the range of $0.84\ \text{GPa} \le P \le 1.23$ GPa, we found that the NQR spectra consist of both narrow and broad peaks (see Supplementary Fig. 7), indicating the coexistence of the commensurate and incommensurate CDWs. Then, there will be a large number of CDW domain walls between the commensurate and incommensurate CDWs in this pressure region. The enhanced interaction and scattering at the domain walls can strongly affect the superconductivity[32,43], which is likely responsible for the inhomogeneous superconductivity, as we found (see Supplementary Fig. 8 for the comparison between the commensurate CDW volume fraction and the superconducting transition width).

A commensurate-to-incommensurate transition with increasing pressures, as we found, was recently proposed theoretically[36], but a superimposed SoD and TrH pattern was not predicted. In CsV_3Sb_5, instead of electron–phonon coupling, electron correlations were suggested to be an important factor in forming the CDW order[27]. Most interestingly, the incommensurate modulation was also reported in Sn-doped CsV_3Sb_5[44]. Then, one possible scenario is that the ordering wave vector connects parts of the Fermi surface or the hot spots. Also, with increasing pressure, due to the change of the Fermi surface, the ordering wave vector gradually becomes incommensurate. Such a scenario was proposed for the CDW order in cuprates, and the wave vector was found to have a monotonous doping dependence[45]. It would be interesting to measure the doping dependence of the wave vector by the high-pressure X-ray scattering.

Possible CDW quantum critical point

Next, we turn to the fluctuations above T_{CDW}. By fitting the ^{121}Sb2 and ^{123}Sb2 spectra with the Lorentz function (see Supplementary Fig. 9 for ^{123}Sb-NQR spectra of the Sb2 site), we deduced the linewidth $\delta\nu^{121}$ and $\delta\nu^{123}$ at various pressures as shown in Fig. 5a, b, respectively. Both $\delta\nu^{121}$ and $\delta\nu^{123}$ increase with decreasing temperature until $T \sim T_{CDW}$, indicating the existence of the short-range CDW order due to CDW fluctuations pinned by quenched disorders, which was also observed in 2H-$NbSe_2$ and underdoped cuprate $YBa_2Cu_3O_y$[46–48]. Our observation is consistent with the recent X-ray scattering and specific heat measurements at ambient pressure, which also show the existence of a short-range CDW order above T_{CDW}[49]. Moreover, we find that the temperature dependence of $\delta\nu$ also follows the Curie–Weiss behavior as observed in $YBa_2Cu_3O_y$[50] and fits both $\delta\nu^{121}$ and $\delta\nu^{123}$

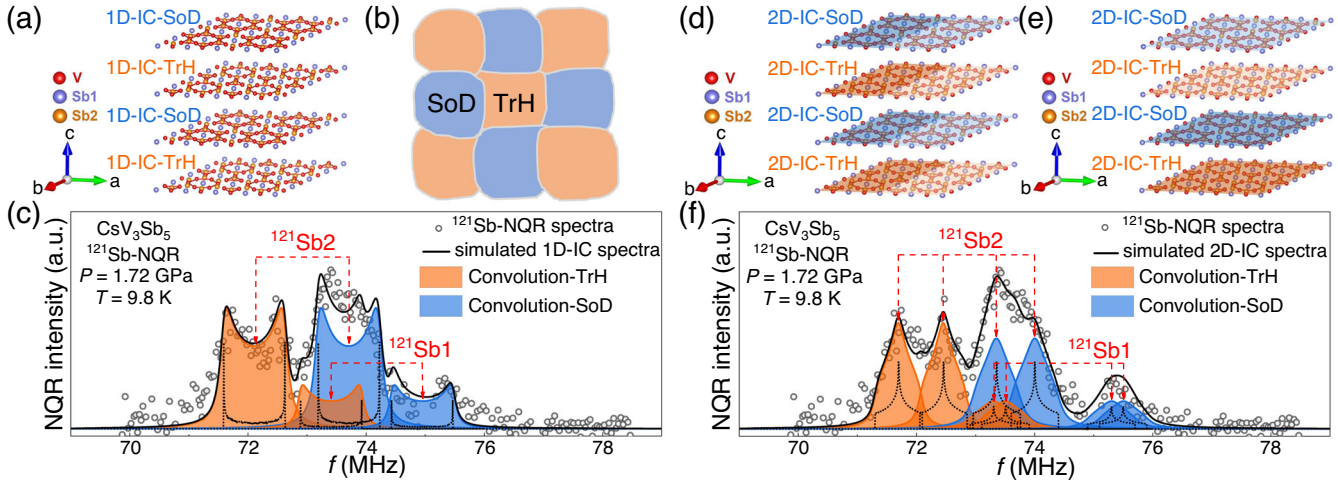

Fig. 4 Simulation of ^{121}Sb-NQR spectrum at $P = 1.72$ GPa. **a** and **b** display the two possible CDW patterns with a one-dimensional (1D) incommensurate (IC) modulation, in which **a** represents the superimposed SoD and TrH pattern stacking along the *c*-axis and **b** represents the coexistence of SoD and TrH domains, respectively. **d** and **e** illustrate the superimposed two-dimensional (2D) incommensurate SoD and TrH pattern with an additional charge modulation along the *a*-axis and *c*-axis, respectively. The gray level represents the charge density. **c** and **f** show the comparison of the ^{121}Sb-NQR spectra at $P = 1.72$ GPa (gray circle), the simulated incommensurate spectra (black dotted line) and the calculated convolution (orange area for TrH pattern and blue area for SoD pattern) for 1D and 2D incommensurate CDW modulations (details about NQR spectra simulation are present in Supplementary Note 5), respectively. The peaks corresponding to Sb1 and Sb2 sites are marked by the red dashed arrows.

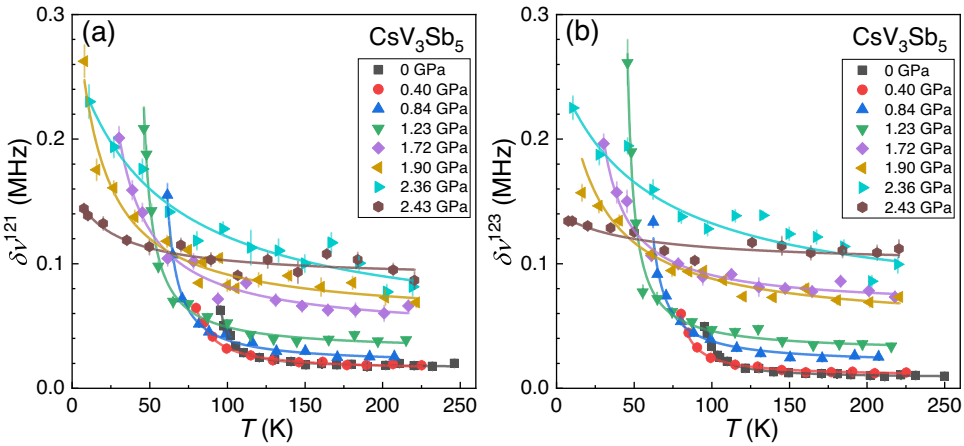

Fig. 5 The NQR linewidth. **a** and **b** show the full-width at half-maximum (FWHM) $\delta\nu$ of $^{121/123}$Sb2-NQR spectra at various pressures. The solid lines are Curie–Weiss fits, and the obtained θ values are plotted in Fig. 6. Error bars are s.d. in the fits of the NQR spectra.

by the Curie–Weiss formula as,

$$\delta\nu^{121,123}(T) = \frac{A^{121,123}}{T - \theta^{121,123}} + C^{121,123} \quad (1)$$

where A represents the amplitude of the Curie–Weiss fit, and C is a constant. As shown in Fig. 5, both $\delta\nu^{121}$ and $\delta\nu^{123}$ are fitted very well, and the obtained $^{121}\theta$ and $^{123}\theta$ are plotted in the phase diagram (see red triangles in Fig. 6). Most surprisingly, we find that both $^{121}\theta$ and $^{123}\theta$ are very close to T_{CDW} from the ambient pressure to $P = 1.72$ GPa, indicating a divergent behavior of $\delta\nu$. Therefore, our results suggest that the NQR line broadening approaching T_{CDW} is related to the CDW fluctuations. There is no present theory giving the quantitative relationship between the CDW susceptibility and the NQR linewidth $\delta\nu$; however, in analogy with the magnetic and nematic quantum phase transitions[7,8], we can take θ as an indicator of the QCP. If $\theta = 0$, it means that the CDW susceptibility diverges at $T \to 0$, indicating a CDW QCP. As shown in Fig. 6, both $^{121}\theta$ and $^{123}\theta$ are almost zero at $P_c \sim 1.9$ GPa, suggesting a CDW QCP at this pressure. We note that T_c reaches the maximum at P_c, implying the possible relationship between CDW fluctuations and the superconductivity. In order to make a firm conclusion, it will be important to make sure whether the CDW transition is of second order at $P > 1.72$ GPa, and whether the CDW QCP is beneath the superconducting dome[9,51].

Spin fluctuations

Lastly, we tried to obtain more information about fluctuations by measuring the spin-lattice relaxation rate $1/T_1$ at both ^{121}Sb2 and ^{123}Sb2 sites at various pressures, as shown in Fig. 7. At all pressures, $1/T_1T$ increases with decreasing temperature toward T_{CDW}. To further show the evolution of $1/T_1T$, we make a contour plot in Fig. 6. $1/T_1T$ is almost identical for $P < 1.72$ GPa, but starts to be enhanced from $P = 1.9$ GPa after the full suppression of the CDW order, which shows a totally different behavior comparing to the NQR line broadening (see Fig. 5). The nuclear spin-lattice relaxation rate $1/T_1$ is mainly composed of two contributions including magnetic interaction and quadrupole interaction. If the quadrupole relaxation process

is predominant, the $1/T_1$ ratio between ^{121}Sb and ^{123}Sb is expected to be $[^{121}Q^2(2\cdot{}^{121}I+3)/{}^{121}I^2(2\cdot{}^{121}I-1)]/[^{123}Q^2(2\cdot{}^{123}I+3)/{}^{123}I^2(2\cdot{}^{123}I-1)]=1.43$[52], in which $^{121}Q=-0.53\times10^{-24}$ cm^2 and $^{123}Q=-0.68\times10^{-24}$ cm^2 are taken. If the magnetic relaxation process is predominant, the $1/T_1$ ratio between ^{121}Sb and ^{123}Sb is expected to be $(^{121}\gamma/{}^{123}\gamma)^2=3.41$, in which $^{121}\gamma=10.189$ MHz/T and $^{123}\gamma=5.51756$ MHz/T are taken. As shown in Fig. 8, the $1/T_1$ ratio $^{123}T_1/{}^{121}T_1$ is close to 3.41 for all pressures, indicating that $1/T_1T$ is mainly contributed by spin fluctuations. Therefore, our results suggest the existence of spin correlations in CsV_3Sb_5. With increasing pressure, the spin correlations are significantly enhanced after the complete suppression of CDW order. More interestingly, as reported by previous transport studies, T_c does not drop rapidly for $P>1.9$ GPa (see Supplementary Fig. 10 for the complete phase diagram)[31,32]. Our results suggest that the superconductivity is sustained by the spin fluctuations at high pressures, which seems to be consistent with recent theoretical studies[36,38]. In passing, we also note that a new superconducting state arises above $P\sim15$ GPa with the pressure further increasing[33,34]. Whether spin fluctuations still play a role for such a higher pressure phase needs high-pressure NMR measurements by using diamond anvils to clarify.

In conclusion, we have presented the systematic $^{121/123}$Sb-NQR measurements on CsV_3Sb_5 under hydrostatic pressures. We found that the CDW structure gradually changes from a commensurate SoD pattern at ambient pressure to a superimposed incommensurate SoD and TrH pattern at $P=1.72$ GPa. Above T_{CDW}, we find that the linewidth of NQR spectra increases with decreasing temperature, indicating the existence of CDW fluctuations pinned by quenched disorders. The linewidth shows a Curie–Weiss

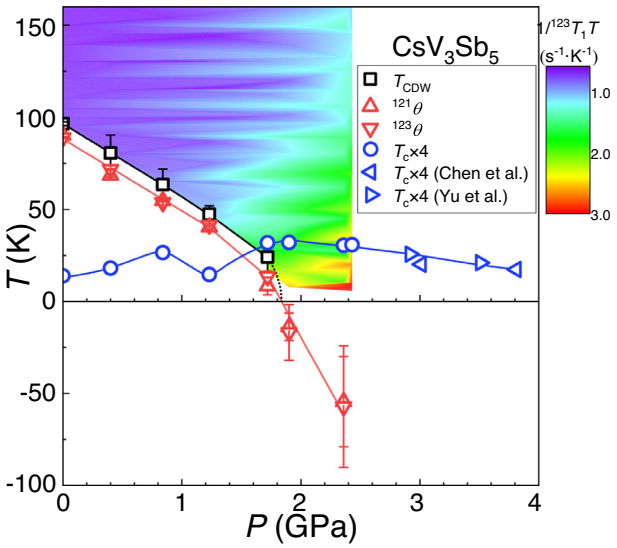

Fig. 6 The obtained phase diagram of CsV_3Sb_5. The black square is the CDW transition temperature T_{CDW} determined by the temperature dependence of Sb2-NQR spectral intensity (see Supplementary Fig. 4). The blue circle is the superconducting transition temperature $T_c\times4$ obtained in this work. The blue triangle is $T_c\times4$ taken from previous transport measurements[31,32]. The red triangle is the obtained $^{121/123}\theta$ from the Curie–Weiss fitting in Fig. 5. For $P=2.43$ GPa, $\delta\nu$ has a very weak temperature dependence, which leads to a large error bar ~ 100 K from the Curie–Weiss fitting. So we did not plot $^{121/123}\theta$ at $P=2.43$ GPa in the phase diagram. Colors in the normal state represent the evolution of the $1/T_1T$ of ^{123}Sb2. Solid and dashed lines are guides to the eye. The error bar for T_{CDW} represents the temperature interval in measuring the NQR spectra (see Supplementary Fig. 4).

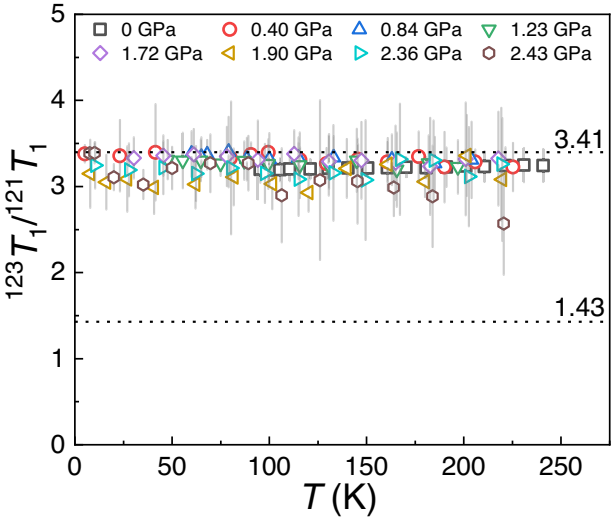

Fig. 8 Temperature dependence of the $1/T_1$ ratio $^{123}T_1/{}^{121}T_1$. The horizontal dashed lines represent purely magnetic fluctuations (ratio = 3.41) and EFG fluctuations (ratio = 1.43), respectively. Error bars are s.d. in the fits of the nuclear magnetization recovery curve.

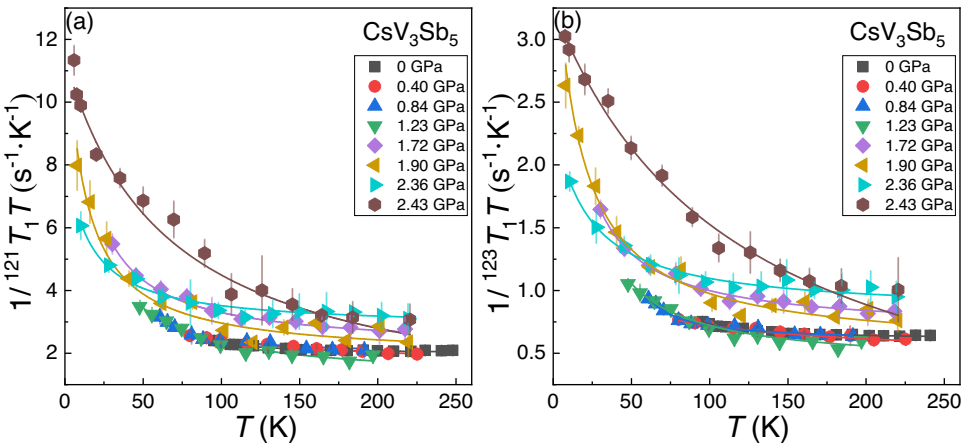

Fig. 7 The quantity $1/T_1T$ of $^{121/123}$Sb at Sb2 cite. a and **b** are temperature-dependent $1/{}^{121}T_1T$ and $1/{}^{123}T_1T$ measured at the Sb2 site under various pressures. Solid lines are guides to the eye. Error bars are s.d. in the fits of the nuclear magnetization recovery curve.

temperature dependence and tends to diverge at $P_c \sim 1.9$ GPa, where T_c shows the maximum. Spin fluctuations are enhanced for $P \geqslant P_c$, which is probably responsible for the slow decrease of T_c at high pressures. Our results reveal the evolution of CDW structure and an emerged CDW QCP with increasing hydrostatic pressures, providing new insight into the superconducting pairing mechanism in CsV_3Sb_5.

METHODS

Sample preparation and NQR measurement

Single-crystal CsV_3Sb_5 was synthesized by the self-flux method[12]. The typical size of the single crystal is around $3 \times 2 \times 0.1$ mm. Several single crystals were mounted inside a piston-cylinder pressure cell made of CuBe alloy. To maintain consistency and ensure the number of quenched disorders remains unchanged, all measurements were conducted on the same single crystals.

The NQR measurements were performed with a phase-coherent pulsed NQR spectrometer. The $^{121/123}$Sb-NQR spectra were acquired by sweeping the frequency point by point and integrating the spin-echo signal. Since the EFG principal axis of $^{121/123}$Sb is along the *c*-axis[28], we stack the CsV_3Sb_5 single-crystal flakes along the *c* direction to obtain a better NQR signal. The nuclear spin-lattice relaxation rate $1/T_1$ was measured by the saturation-recovery method. The $^{121}T_1$ was obtained by fitting the nuclear magnetization $M(t)$ with $1 - M(t)/M(0) = \frac{3}{28}\exp(-3t/T_1) + \frac{25}{28}\exp(-10t/T_1)$ and $^{123}T_1$ was fitted by $1 - M(t)/M(0) = \frac{9}{97}\exp(-3t/T_1) + \frac{16}{97}\exp(-10t/T_1) + \frac{72}{97}\exp(-21t/T_1)$, where $M(0)$ and $M(t)$ are the nuclear magnetization respectively at thermal equilibrium and time t after the comb pulse.

High-pressure NQR measurement

We used a commercial BeCu/NiCrAl clamp cell from C&T Factory Co., Ltd. (Japan) and Daphne oil 7373 as a transmitting medium[53]. When we applied pressure above 1.7 GPa, we heated the pressure cell up to 315 K to prevent the solidification of the pressure medium Daphne 7373[53]. Although care has been taken, there is still a possibility that the pressure might be uniaxial at higher pressures, which could broaden the NQR lines at high temperatures, as shown in Fig. 5. For 0.4 GPa $\leq P \leq$ 2.36 GPa, the applied pressure has been calibrated by the NQR frequency $^{63}\nu_Q$ of Cu_2O[54,55]. The Cu_2O powder and single-crystal CsV_3Sb_5 were placed together inside the NQR coil. There is a pressure deficit from room temperature to low temperature due to the solidification of Daphne oil 7373[53], so the pressure cell was pressurized at room temperature, and the NQR frequency of $^{63}\nu_Q$ was measured at $T \sim 5$ K (see Supplementary Fig. 1). The ν_q of Sb2 shows a linear pressure dependence (see Supplementary Fig. 2d). For $P = 2.43$ GPa, the applied pressure was obtained by the value of ν_q at $T = 100$ K.

DATA AVAILABILITY

The data that support the findings of this study are available from the corresponding authors upon reasonable request.

Received: 26 December 2022; Accepted: 24 April 2023;
Published online: 11 May 2023

REFERENCES

1. Keimer, B., Kivelson, S. A., Norman, M. R., Uchida, S. & Zaanen, J. From quantum matter to high-temperature superconductivity in copper oxides. *Nature* **518**, 179–186 (2015).
2. Chu, J. H., Kuo, H. H., Analytis, J. G. & Fisher, I. R. Divergent nematic susceptibility in an iron arsenide superconductor. *Science* **337**, 710–712 (2012).
3. Wu, T. et al. Magnetic-field-induced charge-stripe order in the high-temperature superconductor YBa_2Cu_3Oy. *Nature* **477**, 191–194 (2011).
4. Stewart, G. R. Heavy-fermion systems. *Rev. Mod. Phys.* **56**, 755 (1984).
5. Lee, P. A., Nagaosa, N. & Wen, X. G. Doping a Mott insulator: physics of high-temperature superconductivity. *Rev. Mod. Phys.* **78**, 17 (2006).
6. Stewart, G. R. Superconductivity in iron compounds. *Rev. Mod. Phys.* **83**, 1589 (2011).
7. Hashimoto, K. et al. A sharp peak of the zero-temperature penetration depth at optimal composition in $BaFe_2(As_{1-x}P_x)_2$. *Science* **336**, 1554–1557 (2012).
8. Zhou, R. et al. Quantum criticality in electron-doped $BaFe_{2-x}Ni_xAs_2$. *Nat. Commun.* **4**, 2265 (2013).
9. Wang, C. G. et al. Electron mass enhancement near a nematic quantum critical point in $NaFe_{1-x}Co_xAs$. *Phys. Rev. Lett.* **121**, 167004 (2018).
10. Luo, J. et al. Tuning the distance to a possible ferromagnetic quantum critical point in $A_2Cr_3As_3$. *Phys. Rev. Lett.* **123**, 047001 (2019).
11. Gruner, T. et al. Charge density wave quantum critical point with strong enhancement of superconductivity. *Nat. Phys.* **13**, 967–972 (2017).
12. Ortiz, B. R. et al. New kagome prototype materials: discovery of KV_3Sb_5, RbV_3Sb_5, and CsV_3Sb_5. *Phys. Rev. Mater.* **3**, 094407 (2019).
13. Ortiz, B. R. et al. CsV_3Sb_5: a Z_2 topological kagome metal with a superconducting ground state. *Phys. Rev. Lett.* **125**, 247002 (2020).
14. Hu, Y. et al. Topological surface states and flat bands in the kagome superconductor CsV_3Sb_5. *Sci. Bull.* **67**, 495–500 (2020).
15. Kang, M. et al. Twofold van Hove singularity and origin of charge order in topological kagome superconductor CsV_3Sb_5. *Nat. Phys.* **18**, 301–308 (2022).
16. Hu, Y. et al. Rich nature of Van Hove singularities in Kagome superconductor CsV_3Sb_5. *Nat. Commun.* **13**, 2220 (2022).
17. Jeong, M. Y. et al. Crucial role of out-of-plane Sb *p* orbitals in Van Hove singularity formation and electronic correlations in the superconducting kagome metal CsV_3Sb_5. *Phys. Rev. B* **105**, 235145 (2022).
18. Hao, Z. Y. et al. Dirac nodal lines and nodal loops in the topological kagome superconductor CsV_3Sb_5. *Phys. Rev. B* **106**, L081101 (2022).
19. Feng, X. L., Jiang, K., Wang, Z. Q. & Hu, J. P. Chiral flux phase in the kagome superconductor AV_3Sb_5. *Sci. Bull.* **66**, 1384–1388 (2021).
20. Wang, Z. W. et al. Electronic nature of chiral charge order in the kagome superconductor CsV_3Sb_5. *Phys. Rev. B* **104**, 075148 (2021).
21. Guo, C. Y. et al. Switchable chiral transport in charge-ordered kagome metal CsV_3Sb_5. *Nature* **611**, 461–466 (2022).
22. Denner, M. M., Thomale, R. & Neupert, T. Analysis of charge order in the kagome metal AV_3Sb_5 (A= K, Rb, Cs). *Phys. Rev. Lett.* **127**, 217601 (2021).
23. Scammell, H. D., Ingham, J., Li, T. & Sushkov, O. P. Chiral excitonic order from twofold van Hove singularities in kagome metals. *Nat. Commun.* **14**, 605 (2023).
24. Nie, L. P. et al. Charge-density-wave-driven electronic nematicity in a kagome superconductor. *Nature* **604**, 59–64 (2022).
25. Khasanov, R. et al. Time-reversal symmetry broken by charge order in CsV_3Sb_5. *Phys. Rev. Res.* **4**, 023244 (2022).
26. Hu, Y. et al. Time-reversal symmetry breaking in charge density wave of CsV_3Sb_5 detected by polar Kerr effect. Preprint at https://arxiv.org/abs/2208.08036 (2022).
27. Li, H. X. et al. Observation of unconventional charge density wave without acoustic phonon anomaly in kagome superconductors *AV*3Sb5 (*A* = Rb, Cs). *Phys. Rev. X* **11**, 031050 (2021).
28. Luo, J. et al. Possible star-of-David pattern charge density wave with additional modulation in the kagome superconductor CsV_3Sb_5. *npj Quantum Mater.* **7**, 30 (2022).
29. Gupta, R. et al. Two types of charge order with distinct interplay with superconductivity in the kagome material CsV_3Sb_5. *Commun. Phys.* **5**, 232 (2022).
30. Lin, Y. P. & Nandkishore, R. M. Multidome superconductivity in charge density wave kagome metals. *Phys. Rev. B* **106**, L060507 (2022).
31. Chen, K. Y. et al. Double superconducting dome and triple enhancement of T_c in the kagome superconductor CsV_3Sb_5 under high pressure. *Phys. Rev. Lett.* **126**, 247001 (2021).
32. Yu, F. H. et al. Unusual competition of superconductivity and charge-density-wave state in a compressed topological kagome metal. *Nat. Commun.* **12**, 3645 (2021).
33. Zhang, Z. et al. Pressure-induced reemergence of superconductivity in the topological kagome metal CsV_3Sb_5. *Phys. Rev. B* **103**, 224513 (2021).
34. Chen, X. et al. Highly robust reentrant superconductivity in CsV_3Sb_5 under pressure. *Chinese Phys. Lett.* **38**, 057402 (2021).
35. Zheng, L. X. et al. Emergent charge order in pressurized kagome superconductor CsV_3Sb_5. *Nature* **611**, 682–687 (2022).
36. Tazai, R., Yamakawa, Y., Onari, S. & Kontani, H. Mechanism of exotic density-wave and beyond-Migdal unconventional superconductivity in kagome metal AV_3Sb_3 (A = K, Rb, Cs). *Sci. Adv.* **8**, eabl4108 (2022).
37. Wang, C. Z., Liu, S. Y., Jeon, H., Jia, Y. & Cho, J. H. Charge density wave and superconductivity in the kagome metal CsV_3Sb_5 around a pressure-induced quantum critical point. *Phys. Rev. Mater.* **6**, 094801 (2022).

38. Bai, X. C. et al. Effective six-band model and unconventional spin-singlet pairing in Kagome superconductor CsV_3Sb_5. *New J. Phys.* **24**, 123016 (2022).
39. Mu, C. et al. S-wave superconductivity in kagome metal CsV_3Sb_5 revealed by $^{121/123}$Sb NQR and ^{51}V NMR measurements. *Chinese Phys. Lett.* **38**, 077402 (2021).
40. Blinc, R. & Apih, T. NMR in multidimensionally incommensurate and CDW systems. *Prog. Nucl. Magn. Reson. Spectrosc.* **41**, 49–82 (2002).
41. Hu, Y. et al. Coexistence of trihexagonal and star-of-David pattern in the charge density wave of the kagome superconductor AV_3Sb_5. *Phys. Rev. B* **106**, L241106 (2022).
42. Li, H. X. et al. Discovery of conjoined charge density waves in the kagome superconductor CsV_3Sb_5. *Nat. Commun.* **13**, 6348 (2022).
43. Lee, K. et al. Metal-to-insulator transition in Pt-doped $TiSe_2$ driven by emergent network of narrow transport channels. *npj Quantum Mater.* **6**, 8 (2021).
44. Kautzsch, L. et al. Incommensurate charge-stripe correlations in the kagome superconductor $CsV_3Sb_{5-x}Sn_x$. Preprint at https://arxiv.org/abs/2207.10608v1 (2022).
45. Comin, R. & Damascelli, A. Resonant x-ray scattering studies of charge order in cuprates. *Annu. Rev. Condens. Matter Phys.* **7**, 369–405 (2016).
46. Berthier, C., Jerome, D. & Molinie, P. NMR study on a 2H-$NbSe_2$ single crystal: a microscopic investigation of the charge density waves state. *J. Phys. C: Solid State Phys.* **11**, 797–814 (1978).
47. Ghoshray, K. et al. ^{93}Nb NMR study of the charge density wave state in $NbSe_2$. *J. Phys.: Condens. Matter* **21**, 155701 (2009).
48. Wu, T. et al. Incipient charge order observed by NMR in the normal state of $YBa_2Cu_3O_y$. *Nat. Commun.* **6**, 6438 (2015).
49. Chen, Q., Chen, D., Schnelle, W., Felser, C. & Gaulin, B. D. Charge density wave order and fluctuations above T_{CDW} and below superconducting T_c in the kagome metal CsV_3Sb_5. *Phys. Rev. Lett.* **129**, 056401 (2022).
50. Vinograd, I. et al. Nuclear magnetic resonance study of charge density waves under hydrostatic pressure in $YBa_2Cu_3O_y$. *Phys. Rev. B* **100**, 094502 (2019).
51. Shibauchi, T., Carrington, A. & Matsuda, Y. A quantum critical point lying beneath the superconducting dome in iron pnictides. *Annu. Rev. Condens. Matter Phys.* **5**, 113–135 (2014).
52. Kitagawa, S., Ishida, K., Nakano, K., Yajima, T. & Kageyama, H. s-wave superconductivity in superconducting $BaTi_2Sb_2O$ revealed by $^{121/123}$Sb-NMR/nuclear quadrupole resonance measurements. *Phys. Rev. B* **87**, 060510 (2013).
53. Yokogawa, K., Murata, K., Yoshino, H. & Aoyama, S. Solidification of high-pressure medium Daphne 7373. *Jpn. J. Appl. Phys.* **46**, 3636 (2007).
54. Reyes, A. P., Ahrens, E. T., Heffner, R. H., Hammel, P. C. & Thompson, J. D. Cuprous oxide manometer for high-pressure magnetic resonance experiments. *Rev. Sci. Instrum.* **63**, 3120 (1992).
55. Kitagawa, K. et al. Space efficient opposed-anvil high-pressure cell and its application to optical and NMR measurements up to 9 GPa. *J. Phys. Soc. Jpn.* **79**, 024001 (2010).

ACKNOWLEDGEMENTS

This work was supported by the National Natural Science Foundation of China (Grant Nos. 11974405, Nos. 11674377, Nos. 11634015, Nos. 51771224, Nos. 61888102, and Nos. 11904023), the National Key Research and Development Projects of China (Grant Nos. 2022YFA1403400, Nos. 2018YFA0305800, and 2019YFA0308500), the Strategic Priority Research Program of the Chinese Academy of Sciences (Grant Nos. XDB33010100 and Nos. XDB33030100) and the Interdisciplinary program of Wuhan National High Magnetic Field Center (Grant No. WHMFC202126), Huazhong University of Science and Technology. A portion of this work was carried out at the Synergetic Extreme Condition User Facility (SECUF).

AUTHOR CONTRIBUTIONS

The single crystals were grown by Z.Z., H.T.Y., and H.J.G. The NMR measurements were performed by X.Y.F., J.L., J.Y., A.F.F., and R.Z. R.Z. and G.Q.Z. wrote the manuscript with inputs from X.Y.F. All authors have discussed the results and the interpretation.

COMPETING INTERESTS

The authors declare no competing interests.

ADDITIONAL INFORMATION

Supplementary information The online version contains supplementary material available at https://doi.org/10.1038/s41535-023-00555-w.

Correspondence and requests for materials should be addressed to R. Zhou.

Reprints and permission information is available at http://www.nature.com/reprints

Publisher's note Springer Nature remains neutral with regard to jurisdictional claims in published maps and institutional affiliations.